A preliminary version of this manuscript has been presented at the
5th International Symposium on Solar Sailing, (29 July – 2 August 2019, Aachen, Germany).

Effects of optical parameter measurement uncertainties and solar irradiance fluctuations on solar sailing

Lorenzo Niccolai*, Alessandro Anderlini, Giovanni Mengali, Alessandro A. Quarta

Department of Civil and Industrial Engineering, University of Pisa, I-56122 Pisa, Italy

Abstract

The heliocentric orbital dynamics of a spacecraft propelled by a solar sail is affected by some uncertainty sources, including possible inaccuracies in the measurement of the sail film optical properties. Moreover, the solar radiation pressure, which is responsible for the solar sail propulsive acceleration generation, is not time-constant and is subject to fluctuations that are basically unpredictable and superimposed to the well-known 11-year solar activity cycle. In this context, this work aims at investigating the effects of such uncertainties on the actual heliocentric trajectory of a solar sail by means of stochastic simulations performed with a generalized polynomial chaos procedure. The numerical results give an estimation of their impact on the actual heliocentric trajectory and identify whether some of the uncertainty sources are more relevant than others. This is a fundamental information for directing more accurate theoretical and experimental efforts toward the most important parameters, in order to obtain an accurate knowledge of the solar sail thrust vector characteristics and, eventually, of the spacecraft heliocentric position.

Keywords: Solar sail, optical force model, solar irradiance fluctuations, uncertainty quantification

Nomenclature

A	=	sail area, $[\mathrm{m}^2]$
$\boldsymbol{a}$	=	propulsive acceleration vector, $[\mathrm{mm/s}^2]$
a_r, a_θ	=	propulsive acceleration components, $[\mathrm{mm/s}^2]$
B	=	non-Lambertian coefficient
b_1, b_2, b_3	=	optical force model coefficients, see Eqs. (6)–(8)
M	=	mean value
m	=	total spacecraft mass, [kg]
$\hat{\boldsymbol{n}}$	=	normal unit vector
P	=	solar radiation pressure, $[\mu\mathrm{Pa}]$
r	=	Sun-spacecraft distance, [au]
$\hat{\boldsymbol{r}}$	=	Sun-spacecraft unit vector
S_i	=	Sobol index associated with uncertain parameter i
s	=	specular reflection coefficient

*Corresponding author

Email addresses: lorenzo.niccolai@ing.unipi.it (Lorenzo Niccolai), alessandro.anderlini@ing.unipi.it (Alessandro Anderlini), g.mengali@ing.unipi.it (Giovanni Mengali), a.quarta@ing.unipi.it (Alessandro A. Quarta)

Published in Advances in Space Research, Vol. 67, No. 9, May 2021, pp. 2784–2794. doi: https://doi.org/10.1016/j.asr.2019.11.037

t	=	time, [days]
u, v	=	spacecraft velocity components, [km/s]
W	=	total solar irradiance, [W/m^2]
α	=	pitch angle, [deg]
β	=	lightness number
ϵ	=	emissivity coefficient
θ	=	polar angle, [deg]
$\mu_\odot$	=	Sun's gravitational parameter, [km^3/s^2]
ρ	=	reflectivity coefficient
σ	=	standard deviation

Subscripts

$\oplus$	=	value at 1 au from the Sun
0	=	initial conditions
b	=	back sail surface
f	=	front sail surface

Accent

$\cdot$	=	time derivative

Acronyms

gPC	=	generalized polynomial chaos
PDF	=	probability density function
TSI	=	total solar irradiance

1. Introduction

A solar sail is a thin reflective membrane capable of generating propulsive acceleration without any propellant consumption, by exploiting the solar radiation pressure exerted by the incoming photons from the Sun [64, 33]. The propellantless working principle of a solar sail enables many fascinating advanced mission applications, such as heliocentric phasing [48, 3], pole-sitter missions [20, 21], displaced non-Keplerian orbits [15], sample return from asteroids [45] or inner planets [23], outer Solar System exploration [34, 2], H-reversal trajectories [66] , and other futuristic scenarios [47, 49, 10, 9].

In a preliminary design phase of a solar sail-based mission, the trajectory analysis is usually performed with the aid of suitable deterministic models, capable of estimating the solar sail thrust vector in a compact analytical form [16]. A very common yet simplified tool is the ideal force model, which uses a perfectly flat sail and assumes all photons impinging on its surface to be specularly reflected, in such a way that the propulsive acceleration only depends on the Sun-sail distance, the area-to-mass ratio, and the sail attitude [33]. In a preliminary mission phase an ideal model (possibly with a smaller sail area for contingency purposes) is often sufficient. More detailed analyses require a force model that takes into account the actual optical properties of the sail film, that is, its specular and diffuse reflection, and the photon emission. Such an optical model is based on the original experimental tests that date back to 1978 [64], at the time when NASA was planning a solar sail rendezvous mission with Halley's comet. More recently, [19] and [18] have published the results of a new experimental campaign, aimed at measuring the optical properties of an aluminum-coated sail. Both the ideal and the optical force models neglect the sail billowing effect and the degradation process of the sail film [8, 7, 22].

In some cases the optical force model may not be accurate enough even in a preliminary mission design phase, especially when the optical properties of the sail film are not precisely estimated. In fact, an accurate knowledge of the sail thrust vector is required in many mission scenarios, even though it is usually difficult to obtain, since significant experimental efforts are necessary to get the actual (in-flight) values of the reflective film optical coefficients [37]. A further uncertainty source for a solar sail trajectory design is given by the

time fluctuations of solar properties. In fact, the solar radiation pressure is generated by the power flux of the incoming photons from the Sun (that is, the solar irradiance). The total solar irradiance (TSI) undergoes a 11-year solar activity cycle, but it is also characterized by non-negligible random components [29]. Indeed, the magnitude of the fluctuations typically amounts to $0.1\% - 0.2\%$ of its mean value, with peaks above 3% [13, 11]. Although such variations are three order of magnitudes smaller than those of the solar wind dynamic pressure [56], the preliminary results provided by [59, 60] recommend to take them into account in missions requiring an accurate targeting capability.

The uncertainty in the thrust vector characteristics could be overcome with the procedure proposed by [50], who suggested to generate a collinear, artificial, equilibrium point in the Sun-Earth gravitational field by means of a solar sail-based spacecraft whose performance level is theoretically greater than that required to maintain the working orbit. In that case, the required propulsive acceleration is purely radial, that is, the thrust vector is nominally directed along the Sun-spacecraft line. After the sail deployment, on condition that the actual thrust magnitude is larger than that required for orbital maintenance, the solar sail needs to be steered with a suitable control law, such that the mean radial propulsive acceleration complies with the mission requirement, while the mean circumferential propulsive acceleration is kept to zero. This approach is conceptually similar to that proposed by [6], who investigated mission applications in which the effective sail performance is greater than that required by a specific scenario, including heliocentric transfers and hovering above asteroids. However, such a procedure is rather involved and has some physical limitations, and so is hardly applicable in complex missions.

A possible alternative is the use of Electrochromic Coating Systems (ECSs), which may significantly increase the thrust modulation capability of a solar sail. An ECS exploits the property of electrochromic materials [17, 38] to change their reflectivity under the application of a small electric voltage. JAXA's IKAROS mission has demonstrated the effectiveness of an ECS-based attitude control system around the pitch and roll axes [57, 14], and the recent manufacturing of advanced ECSs [24], which exploit the refractive properties of liquid crystals, allows the attitude control system to generate a net torque even about the yaw (that is, the normal) axis. Note that ECSs could be used in principle not only for spacecraft attitude control, but also to obtain a small modulation of the thrust vector [39, 42].

Based on the previous considerations, a quantification of the impact of the thrust vector uncertainty on the solar sail trajectory becomes a fundamental issue from a mission design viewpoint. The aim of this work is to provide a systematic analysis of the uncertainty sources that affect the trajectory of a solar sail, in order to identify those having a significant impact on the mission performance. The results of such analysis could direct further theoretical and experimental efforts toward the most relevant parameters for the trajectory design, thus allowing the least significant ones to be neglected. This preliminary investigation neglects any degradation effect due to space environment and, in general, any change of solar sail film property due to corpuscolar solar radiation. The billowing effects are also neglected, as is suggested by experimental data provided by IKAROS and NEA Scout missions.

Several approaches for uncertainty quantification have been discussed in specialized literature, including linearized propagation models [4], Monte Carlo simulations [5], and differential algebra-based approaches [58]. In this work, a generalized polynomial chaos (gPC) procedure [65] is used, which has proved its effectiveness in different aerospace-related studies [32, 31, 40, 41].

The paper is structured as follows. First, an overview of the sail optical force model is given, along with a report of the recent experimental measurements of the sail reflective film optical parameters. Then, the gPC method is briefly described and applied to the solar sail trajectory design, in order to identify the parameters that have a significative effect on it. The conclusion section summarizes the main outcomes of this work.

2. The role of uncertainties in the optical force model

Consider a solar sail-based spacecraft whose propulsive acceleration constantly lies on the osculating orbital plane, so that the spacecraft propelled trajectory is two-dimensional. In this case, with reference to

Fig. 1, the spacecraft equations of motion can be written in a heliocentric, polar reference frame as

$$\dot{r} = u \tag{1}$$

$$\dot{\theta} = \frac{v}{r} \tag{2}$$

$$\dot{u} = \frac{v^2}{r} - \frac{\mu_\odot}{r^2} + a_r \tag{3}$$

$$\dot{v} = -\frac{u\,v}{r} + a_\theta \tag{4}$$

where r is the Sun-spacecraft distance, θ is the polar angle measured counterclockwise with respect to a fixed direction (usually taken coincident with the Sun-spacecraft vector at $t_0 \triangleq 0$), u and v are the radial and circumferential velocity components, $\mu_\odot$ is the Sun's gravitational parameter, and the dot symbol denotes a derivative with respect to time. In Eqs. (3) and (4), a_r and a_θ are the radial and circumferential components of the propulsive acceleration vector $\boldsymbol{a}$, respectively, whose expressions depend on the force model used to describe the sail thrust vector.

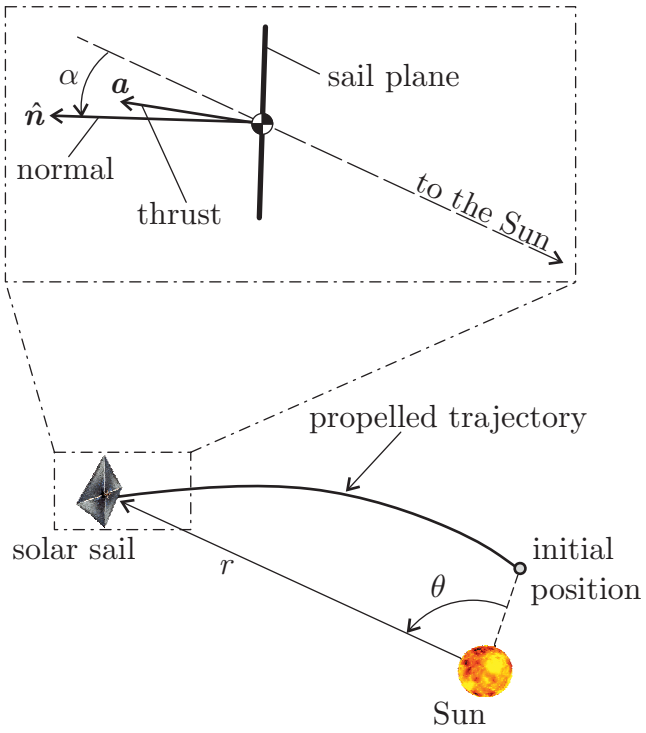

Figure 1: Sketch of the polar reference frame used in the dynamical model.

Using the optical force model [33], $\boldsymbol{a}$ is a function of the amount of photons that are either absorbed, specularly or diffusely reflected, or emitted. More precisely, the propulsive acceleration vector may be written as

$$\boldsymbol{a} = \beta \left(\frac{\mu_\odot}{r^2}\right) \frac{1}{b_1 + b_2 + b_3} \left(\hat{\boldsymbol{r}} \cdot \hat{\boldsymbol{n}}\right) \left\{b_1\, \hat{\boldsymbol{r}} + \left[b_2 \left(\hat{\boldsymbol{r}} \cdot \hat{\boldsymbol{n}}\right) + b_3\right] \hat{\boldsymbol{n}}\right\} \tag{5}$$

where β is the sail lightness number, defined as the ratio of the maximum propulsive acceleration magnitude at a given Sun-spacecraft distance r to the local solar gravitational acceleration, $\hat{\boldsymbol{r}} \triangleq \boldsymbol{r}/r$ is the radial unit vector, and $\hat{\boldsymbol{n}}$ is the unit vector normal to the sail nominal plane in the direction opposite to the Sun, that is, $\hat{\boldsymbol{n}} \cdot \hat{\boldsymbol{r}} \geq 0$. In Eq. (5), $\{b_1,\, b_2,\, b_3\}$ are the sail force coefficients [36], which depend on the optical properties

of the sail film [33], viz.

$$b_1 = \frac{1 - \rho\, s}{2} \tag{6}$$

$$b_2 = \rho\, s \tag{7}$$

$$b_3 = \frac{B_f\, \rho\, (1 - s)}{2} + \frac{(1 - \rho)\, (\epsilon_f\, B_f - \epsilon_b\, B_b)}{2\, (\epsilon_f + \epsilon_b)} \tag{8}$$

where ρ is the reflectivity coefficient, s is the fraction of specularly reflected photons, B_f (or B_b) is the front (or back) non-Lambertian coefficient, and ϵ_f (or ϵ_b) is the front (or back) emissivity of the sail surface. The ideal force model is recovered by simply setting $\rho = s = 1$, which implies $b_1 = b_3 = 0$, $b_2 = 1$, and $\hat{\boldsymbol{a}} \equiv \hat{\boldsymbol{n}}$ with $\hat{\boldsymbol{a}} \triangleq \boldsymbol{a} / \|\boldsymbol{a}\|$. When the propulsive acceleration vector $\boldsymbol{a}$ of Eq. (5) is projected along the radial and circumferential direction, the result is

$$a_r = \beta \left(\frac{\mu_\odot}{r^2}\right) \frac{1}{b_1 + b_2 + b_3} \left(b_1\, \cos\alpha + b_2\, \cos\alpha^3 + b_3 \cos\alpha^2\right) \tag{9}$$

$$a_\theta = \beta \left(\frac{\mu_\odot}{r^2}\right) \frac{1}{b_1 + b_2 + b_3} \left(b_2\, \cos\alpha^2\, \sin\alpha + b_3 \cos\alpha\, \sin\alpha\right) \tag{10}$$

where the pitch angle $\alpha \in [-90, 90]\,\mathrm{deg}$ is defined as the angle between $\hat{\boldsymbol{r}}$ and $\hat{\boldsymbol{n}}$, see Fig. 1. The next discussion concentrates on the uncertain terms in Eq. (5) or, equivalently, in Eqs. (9) and (10).

2.1. Statistical model of the solar radiation pressure

The first source of uncertainty in the propulsive acceleration is given by the lightness number β that, according to [33], can be written as a function of the solar radiation pressure as

$$\beta = \frac{2\, P_\oplus\, A}{m\, \mu_\odot / r_\oplus^2}\, (b_1 + b_2 + b_3) \tag{11}$$

where A is the sail area, m is the total spacecraft mass, and $P_\oplus$ is the solar radiation pressure at a reference distance $r = r_\oplus \triangleq 1\,\mathrm{au}$, that is

$$P_\oplus = W_\oplus / c \tag{12}$$

in which $W_\oplus$ is the TSI at $r = r_\oplus$, and c is the speed of light.

Environmental uncertainties affect the propulsive acceleration vector through the term $W_\oplus$ in Eq. (12). In fact, recent studies and experimental measurements [13, 11] highlight that, despite the TSI is nearly isotropic and its time behaviour is mainly affected by the predictable 11 year-solar activity cycles, the actual value of $W_\oplus$ undergoes non-negligible chaotic short-term fluctuations. Accordingly, $W_\oplus$ may be conservatively thought of as a random variable, whose instantaneous value is independent of the previous values, in analogy with the recent model adopted by [40, 41] for the solar wind dynamic pressure used for a preliminary analysis of the Electric Solar Wind Sail trajectory [62, 63]. The probability density function (PDF) adopted in this work to describe $W_\oplus$ is a Gaussian distribution, which amounts to neglecting the skewness of the TSI distribution, and to approximating its kurtosis with 3. These assumptions are supported by available reports on experimental data [61], according to which the skewness of the observed TSI distribution is on the order of 0.1 only, while the kurtosis index is about 8, which is larger than that predicted by a Gaussian model, thus implying that the experimental measurements are more concentrated around their peak value.

In a preliminary mission analysis phase, $W_\oplus$ is typically taken equal to a mean value of $1365.4\,\mathrm{W/m^2}$. However, the experimental measurements performed by the SORCE mission [51, 30] have recently updated its mean value to $1360.8\,\mathrm{W/m^2}$, with an uncertainty range of about $0.5\,\mathrm{W/m^2}$. A sample of *in-situ* measurements performed by SORCE[1] is reported in Fig. 2. Even though the mean value of $1360.8\,\mathrm{W/m^2}$ obtained by SORCE is considered to be more accurate than the previous $1365.4\,\mathrm{W/m^2}$ [12], it is worth noting that the

[1] See `http://lasp.colorado.edu/home/sorce/data/tsi-data/`. Data retrieved on 28 June 2019.

former corresponds to a quite low solar activity period. For this reason [29] have recently proposed to model $W_\oplus$ as the sum of three contributions, that is, its mean value ($1360.8\,\mathrm{W/m^2}$), to which rapid fluctuations (on the order of $\pm 2.3\,\mathrm{W/m^2}$) and long-term fluctuations (on the order of $\pm 0.8\,\mathrm{W/m^2}$), mostly related to the 11-year solar cycle [11, 28], are both superimposed. In this work, a short-term (or medium-term) duration mission is considered, so that the long-term fluctuations of $W_\oplus$ may be considered to be negligible, which simplifies the problem complexity.

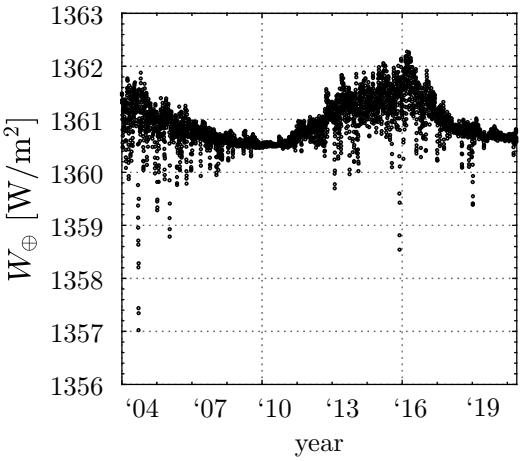

Figure 2: Value of TSI at 1 au measured by SORCE mission from January 2014 to June 2019.

The total standard deviation $\sigma_{W_\oplus}$ of $W_\oplus$ is therefore assumed to be affected by two contributions, that is, i) the standard deviation associated to the uncertain measurements of the mean value; and ii) the contribution given by the short-term (random) fluctuations. However, since the TSI estimates are highly uncertain, other *in-situ* measurements may provide different results when compared to those obtained by the SORCE mission, as is discussed by [11]. Therefore, a safety factor $k = 2$ is here included in the standard deviation, that is

$$\sigma_{W_\oplus} = k\,\sqrt{2.3^2 + 0.5^2}\,\mathrm{W/m^2} \simeq 4.7\,\mathrm{W/m^2} \tag{13}$$

To summarize, $W_\oplus$ is modeled as a Gaussian variable with a mean value of $1360.8\,\mathrm{W/m^2}$ and a standard deviation of $4.7\,\mathrm{W/m^2}$.

2.2. Estimation of sail optical parameters

A first estimate of the sail film optical properties involved in Eqs. (5)–(8) was made by [52], when the Jet Propulsion Laboratory (JPL) was investigating the feasibility of a rendezvous mission with Halley's comet by means of a solar sail-based spacecraft [25]. The proposed mission was eventually canceled, but the experimental results were actually published [64, 33] and reported, for the sake of completeness, in Tab. 1. Substituting these values into Eqs. (6)–(8), the force coefficients become $b_1 = 0.0864$, $b_2 = 0.8272$, and $b_3 = -0.0054$, with $b_1 + b_2 + b_3 = 0.9082$.

Table 1: Optical parameters for a flat solar sail with an optical force model, according to the 1978 measurements by JPL [33].

ρ	s	B_f	B_b	ϵ_f	ϵ_b
0.88	0.94	0.79	0.55	0.05	0.55

[19] revised the original data of 1978, and provided a refinements of some parameters, based on experimental tests performed in 2004, and on theoretical investigations involving the sail membrane behaviour. They state that a 100 nm aluminum coating is sufficient to ensure that the optical properties of the sail film are only influenced by the coating itself, and not by the substrate material, which therefore could

equivalently be either CP1 polyamide, Kapton, or Mylar. The results by [19] are listed in Tab. 2, and the corresponding values of the force coefficients in Eqs. (6)–(8) are amended to $b_1 = 0.0723$, $b_2 = 0.8554$, and $b_3 = -0.0030$, with $b_1 + b_2 + b_3 = 0.9247$.

Table 2: Optical parameters for a flat solar sail with an optical force model, according to the 2015 measurements by NASA [19].

ρ	s	B_f	B_b	ϵ_f	ϵ_b
0.91	0.94	0.79	0.67	0.025	0.27

The results obtained in 2015 were later updated by [18], taking into account further experimental campaigns performed during the preliminary mission design phase of NASA's NEA Scout mission, a rendezvous mission with a near-Earth Asteroid using a solar sail during its cruise phase [35]. In particular, the assumption of flat sail was relaxed by [18], who showed that the presence of millimeter-scale wrinkles can be modeled as a reduction of the specular reflection fraction to a new value of $s = 0.89$, leaving unaffected all of the other parameters in Tab. 2. The corresponding (nominal) values of the optical coefficients are then $b_1 = 0.0950$, $b_2 = 0.8099$, and $b_3 = 0.0150$, with $b_1 + b_2 + b_3 \simeq 0.92$.

Notably, all the experimental measurements performed so far [33, 19, 18], have given a very small value of b_3 coefficient. Such result has supported the introduction of simplifying assumptions in previous works on solar sail trajectory analysis [43], and also suggests that the optical parameters involved in its calculation, that is, the non-Lambertian and the emissivity coefficients (see Eq. (8)), have a very small impact on the characteristics of the propulsive acceleration vector. However, in order to perform a complete and exhaustive analysis, all of the optical parameters will be treated in the following analysis as uncertain parameters, as is done with $W_\oplus$. The uncertain parameters are summarized in Tab. 3, which reports their mean value M and standard deviation σ. The values in Tab. 3 constitute the basis of the statistical estimation of the solar sail heliocentric trajectory discussed in the next section.

Table 3: Mean value M and standard deviation σ of the uncertain parameters involved in solar sail thrust generation [19, 18, 51, 30, 29].

	ρ	s	B_f	B_b	ϵ_f	ϵ_b	$W_\oplus$ [W/m^2]
M	0.91	0.89	0.79	0.67	0.025	0.27	1360.8
σ	0.005	0.045	0.05	0.05	0.005	0.005	4.7

3. Generalized polynomial chaos procedure

The previous model of sail film optical properties and TSI behaviour is now used to quantify the impact of the uncertainties related to these variables on the heliocentric trajectory of a solar sail. For computational purposes, the adopted procedure uses a non-intrusive gPC-based algorithm, which is a spectral projection of a quantity of interest R (considered as a random process) over a known orthogonal polynomial base. More precisely, the formal gPC expansion of R (that is, R_{gPC}) can be written in a compact form as

$$R_{\mathrm{gPC}} = \sum_{j=0}^{P_{\mathrm{tot}}} \lambda_j \Psi_j(\boldsymbol{\xi}) \tag{14}$$

where $\boldsymbol{\xi} \triangleq [\xi_1, .., \xi_N]$ is an N-dimensional vector belonging to the parameter space $\Omega \subseteq \mathbb{R}^N$, whose components are the uncertain parameters. In this analysis, the random process coincides with the Sun-spacecraft distance, that is, $R \equiv r$, and the uncertain parameters are those listed in Tab. 3. Each parameter in Tab. 3 is treated as a random variable independent of all the others, with a Gaussian statistical distribution. The generic PDF of a random parameter ξ_j is denoted as w_j. As will be now clarified, the choice of the PDF influences the polynomial base associated to that variable.

In Eq. (14), $\Psi_j(\boldsymbol{\xi})$ is the gPC multidimensional polynomial base of index j, λ_j is the related Galerkin projection coefficient, and P_{tot} is the truncation order depending on the number of uncertain parameters and on the maximum polynomial basis degree. In this paper we use the so-called "tensor-product" truncation, which means that a polynomial-order bound P is imposed for each single parameter polynomial base, such that $P_{\text{tot}} = (P+1)^N - 1$.

From the orthogonality property of the base, each expansion coefficient λ_j can be computed as

$$\lambda_j = \frac{\langle R, \Psi_j \rangle}{\langle \Psi_j, \Psi_j \rangle} \tag{15}$$

where

$$\langle u, g \rangle = \int_\Omega g(\boldsymbol{\xi})\, u(\boldsymbol{\xi})\, w_{\text{tot}}(\boldsymbol{\xi})\, \mathrm{d}\boldsymbol{\xi} \tag{16}$$

denotes the inner product between two generic functions g and u, with $\mathrm{d}\boldsymbol{\xi} = \prod_{j=1}^{N} \mathrm{d}\xi_j$, while $w_{\text{tot}}(\boldsymbol{\xi})$ is a weight defined as

$$w_{\text{tot}}(\boldsymbol{\xi}) = \prod_{j=1}^{N} w_j(\xi_j) \tag{17}$$

which is simply the product of the PDF w_j associated to the uncertain variable ξ_j. According to the Askey scheme [65], the polynomial family orthogonal to a Gaussian PDF is that of Hermite.

All of the inner products involved in this methodology are computed through Gaussian quadrature formulas using $(P+1)$ nodes per parameter. Therefore, the full N-dimensional tensor-product grid counts $(P+1)^N$ points. Each quadrature point defines a parameter set-up for which the quantity R must be sampled, so that a number of $(P+1)^N$ deterministic evaluations only are sufficient to estimate the dynamic model uncertainties, the mean stochastic value and the standard deviation of $R \equiv r$. A value $P = 4$ was chosen, which corresponds to 5 Gauss-Hermite nodes for each uncertain parameter, that is, $(P+1)^N = 5^3 = 125$.

The procedure described so far, however, can only provide some findings about the global sensitivity of R to all the input uncertainties. A further interesting information is to quantify the effect of each single variable, in order to measure the relative impact of each uncertainty parameter on the resulting output. A possible strategy to obtain such an estimation was proposed by [55]. The essential idea is to express the gPC expansion R_{gPC} as the "ANOVA representation" of a generic function of the vector of uncertain parameters $f(\boldsymbol{\xi})$, viz.

$$R_{\text{gPC}} = f(\boldsymbol{\xi}) = f_0 + \sum_{k=1}^{N} \sum_{\substack{i_1,\ldots,i_k=1 \\ i_1<\ldots<i_k}}^{N} f_{i_1\ldots i_k}(\xi_{i_1}, \ldots, \xi_{i_k}) \tag{18}$$

where $[\xi_{i_1}, \ldots, \xi_{i_k}]$ is a subset of k variables among N, f_0 is the mean value of f, and $f_{i_1\ldots i_k}(\xi_{i_1}, \ldots, \xi_{i_k})$ is its ANOVA expansion term, which can be calculated with the algorithm described by [55]. Because all the terms of the ANOVA representation are orthogonal to the PDF of each variable, it can be shown that the total variance of f may be decomposed as the sum of the variances of all the $f_{i_1\ldots i_k}$ terms, viz.

$$\sigma_f^2 = \sum_{k=1}^{N} \sum_{\substack{i_1,\ldots,i_k=1 \\ i_1<\ldots<i_k}}^{N} \sigma_{i_1\ldots i_k}^2 \tag{19}$$

It is now possible to define the so called "Sobol indexes" (also referred to as "sensitivity indexes") as

$$S_{i_1\ldots i_k} = \frac{\sigma_{i_1\ldots i_k}^2}{\sigma_f^2} \tag{20}$$

where σ_f is given by Eq. (19). From the above definition, it follows that the Sobol indexes are a set of non-negative numbers, ranging between 0 and 1, which quantify how much each single variable subset (of order $k \in [1, N]$) contributes to the total variance of f. In particular, an index equal to 1 indicates that the whole variability of f is due to the considered group of uncertain variables, while a value equal to 0 means

that the function is insensitive to that subset. Finally, according to Eq. (19), the sum of all the indexes is equal to 1, viz.

$$\sum_{k=1}^{N} \sum_{\substack{i_1,\ldots,i_k=1 \\ i_1<\ldots<i_k}}^{N} S_{i_1\ldots i_k} = 1 \tag{21}$$

4. Numerical simulations

The gPC-based procedure discussed in the previous section is now used to quantify the impact of uncertainties (related to the optical properties and the TSI value) on the spacecraft trajectory in a heliocentric two-dimensional mission scenario. The investigation aims at estimating how much an uncertainty on the input parameters (see Tab. 3) affects the Sun-spacecraft distance r, as is illustrated in Fig. 3. The solar sail dynamics is simulated by integrating Eqs. (1)-(4) in double precision using a variable order Adams-Bashforth-Moulton solver scheme [53, 54] with absolute and relative errors of 10^{-12}.

The design parameters of the spacecraft and the solar sail used for the simulations are taken from the NASA NEA Scout mission [46]. In particular, the total spacecraft mass is assumed to be $m = 12\,\mathrm{kg}$, and the sail area is $A = 86\,\mathrm{m}^2$. The nominal lightness number is therefore $\beta \simeq 0.0101$, obtained by substituting the mean values of the uncertain parameters listed in Tab. 3 and the nominal values of the optical coefficients (in the last four columns of Tab. 2) into Eq. (11). The previous value of β constitutes the current state-of-the-art of the solar sail technology, since it is significantly larger than that of IKAROS mission ($\beta \simeq 9 \times 10^{-4}$) and close to that hypothesized for the planned JAXA OKEANOS mission toward the Jupiter's Trojan asteroids, in which $\beta \simeq 0.016$ [44]. In each numerical simulation, the solar sail-based spacecraft initially (at time $t = t_0 \triangleq 0$) covers a heliocentric circular orbit of radius $r_0 = r_\oplus$. This situation corresponds to a spacecraft that leaves the Earth's sphere of influence with zero hyperbolic excess velocity with respect to the planet.

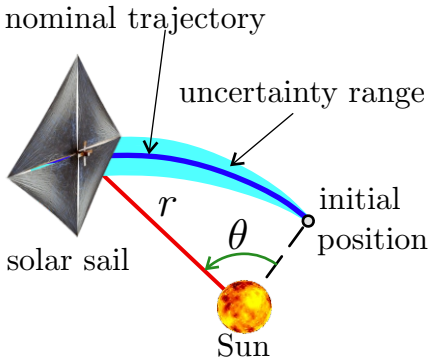

Figure 3: Sketch of the solar sail trajectory with uncertain input parameters.

When $t > t_0$, the sail attitude is maintained fixed in an orbital reference frame. Two cases are first simulated, both being characterized by a propulsive acceleration vector that always belongs to the parking orbit plane, an so generates a two-dimensional propelled trajectory. The first one is a radial thrust case with $\hat{\boldsymbol{n}} \equiv \hat{\boldsymbol{r}}$, which maximizes the propulsive acceleration magnitude at each Sun-spacecraft distance r. In the second case, the pitch angle is set equal to $\alpha = 35\,\mathrm{deg}$, which corresponds to maximizing the circumferential component of the propulsive acceleration a_θ in an ideal force model, and is very close to the maximum value also when an optical force model is adopted, see Eq. (10). In such simulations only the most relevant optical parameters $\{\rho, s\}$ and $W_\oplus$ are taken as uncertain inputs, in order to reduce the computational cost. The non-Lambertian and emissivity coefficients are considered to be constant and equal to their mean values reported in Tab. 3. The last simulation finally assumes a fixed pitch angle $\alpha = 35\,\mathrm{deg}$, but takes into accounts the uncertainties on all the parameters of Tab. 3, in order to check the previous assumption of neglecting the standard deviation of B_f, B_b, ϵ_f, and ϵ_b.

4.1. Case of radial propulsive acceleration

The simulation results of a sail with purely radial propulsive acceleration (case of a Sun-facing sail) and subject to uncertainties on $\{\rho, s, W_\oplus\}$ are shown in Figs. 4 and 5. In particular, Fig. 4 shows the standard deviation σ_r of the Sun-spacecraft distance r, normalized with respect to r itself, as a function of the polar angle $\theta \in [0, 360]$ deg. The latter is measured starting from the Sun-spacecraft line at $t = t_0$. The values of σ_r reported in Fig. 4 are very small, on the order of a few hundredths of percentage point, thus suggesting that the uncertainties associated with $\{\rho, s, W_\oplus\}$ do not significantly affect the trajectory of a spacecraft propelled by a Sun-facing solar sail.

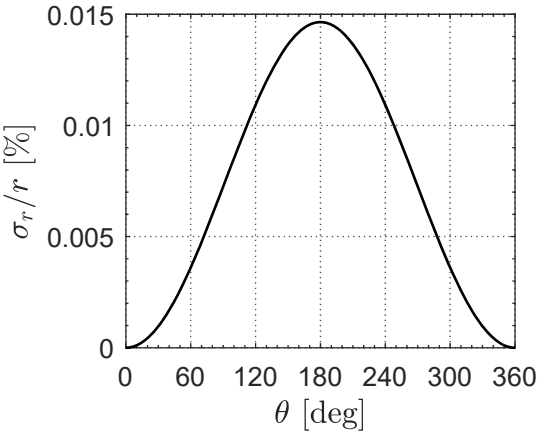

Figure 4: Normalized standard deviation associated with the Sun-spacecraft distance as a function of the polar angle for a Sun-facing sail.

Figure 5 shows the evolution of the Sobol indexes related to the uncertain variables $\{\rho, s, W_\oplus\}$ as a function of $\theta \in [0, 360]$ deg. Firstly, note that the correlation indexes of two or three variables are negligible, since their values are from 4 to 9 order of magnitudes smaller than those associated to a single variable, that is, $S_{\rho s} = S_{\rho W_\oplus} = S_{s W_\oplus} = S_{\rho s W_\oplus} \simeq 0$, see Eq. (20). The indexes associated to single variables, that is, $\{S_\rho, S_s, S_{W_\oplus}\}$, are nearly constant with respect to θ, and their numerical values are comparable, although the index associated to s is the largest one (i.e. $S_s \simeq 0.432$). However, because the uncertainty associated to a radial trajectory is very small, see Fig. 4, the Sobol indexes are of limited interest.

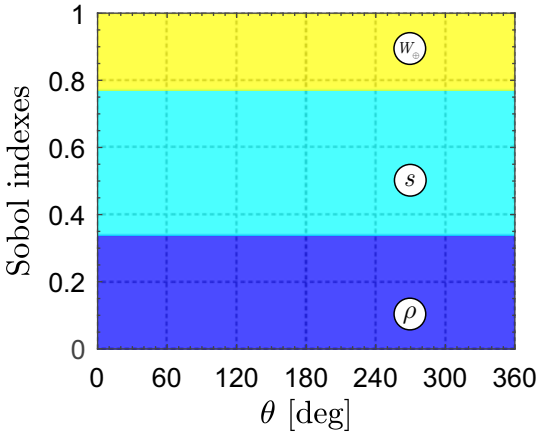

Figure 5: Sobol indexes S_ρ (blue), S_s (cyan), and $S_{W_\oplus}$ (yellow) as a function of the polar angle θ for a Sun-facing sail. Indexes $\{S_{\rho s}, S_{\rho W_\oplus}, S_{s W_\oplus}, S_{\rho s W_\oplus}\}$ are not visible due to their small value.

4.2. Case of maximum circumferential acceleration

Assume now that the propulsive acceleration is at an angle of 35 deg from the radial (Sun-spacecraft) direction. This choice maximizes the circumferential component of the propulsive acceleration [33]. The corresponding results, which take into account the uncertainties associated with $\{\rho, s, W_\oplus\}$, are given in Fig. 6 in terms of uncertainty propagation in the Sun-spacecraft distance r. In particular, the figure reports σ_r as a function of $\theta \in [0,\, 720]$ deg. The uncertainty on r now grows significantly faster than in the radial thrust case, although it remains small (much smaller than 1%). In principle, it is difficult to state if such a deviation is large of small, because it mostly depends on mission requirements. For instance, consider an asteroid rendezvous mission and a Solar System escape mission. In the former case, such a deviation could cause a mission failure, whereas in the latter case it could be nearly negligible. Anyway, the trajectory error can be checked by reducing the uncertainty on solar film properties, either with experimental tests, or using a suitable attitude control.

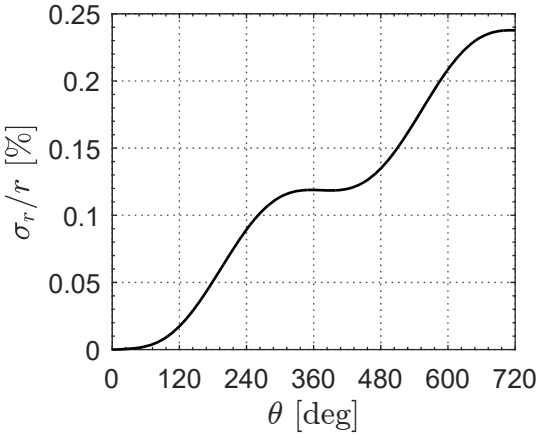

Figure 6: Normalized standard deviation associated with the Sun-spacecraft distance in the case of maximum circumferential acceleration.

The Sobol indexes associated with each of the uncertain variables are shown in Fig. 7 where, similarly to Fig. 5, the indexes $S_{\rho s}$, $S_{\rho W_\oplus}$, $S_{sW_\oplus}$, and $S_{\rho s W_\oplus}$ are not visible because they are several order of magnitudes smaller than those associated with each single variable. By comparing Figs. 6 and 7, it may be concluded that, when the uncertainty on r is not negligible, the most important parameter is s, followed by ρ and $W_\oplus$. This result is probably associated with the larger uncertainty on s, whose standard deviation is about 5% of its mean value, whereas this percentage reduces to 0.5% and 3.4% as long as ρ and $W_\oplus$ are concerned, see Tab. 3. Indeed, the uncertainty on s takes into account the difficulty of determining the specular reflection fraction of the sail coating, and the effects of millimeter-scale wrinkles. However, these preliminary results highlight that a more accurate knowledge of the sail film specular reflection fraction and of the wrinkle effect could significantly increase the computational accuracy of a solar sail trajectory.

4.3. Effect of non-Lambertian and emissivity coefficients

The simulations discussed above neglect the uncertainties on the non-Lambertian coefficients $\{B_f, B_b\}$, and on the emissivity coefficients $\{\epsilon_f, \epsilon_b\}$, since their impact on the heliocentric trajectory was supposed to be small. In this subsection, the latter assumption is removed and all of the uncertain input parameters listed in Tab. 3 are now taken into account. In particular, a pitch angle $\alpha = 35$ deg is chosen, and the uncertainty in the output variable r is calculated at $\theta = \{60,\, 120,\, 180,\, 240,\, 300,\, 360\}$ deg. The numerical results are summarized in Tab. 4, in terms of Sobol indexes associated with each input parameter. Note that the indexes associated with the correlation of two or more variables are not reported, since they are actually negligible compared to those associated with a single variable, as can be concluded by noting that the sum of the Sobol indexes in each row of Tab. 4 is nearly equal to 1.

The most important implication from the data of Tab. 4 is the negligible impact of the uncertainties associated with the non-Lambertian coefficients $\{B_f, B_b\}$ and the emissivity coefficients $\{\epsilon_f, \epsilon_b\}$ on the

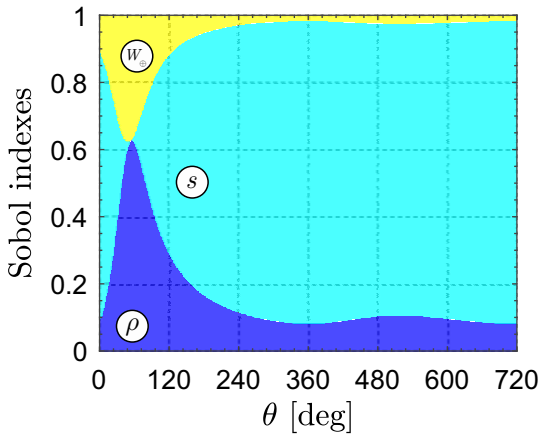

Figure 7: Sobol indexes S_ρ (blue), S_s (cyan), and $S_{W_\oplus}$ (yellow) as a function of the polar angle θ in the case of maximum circumferential acceleration. Indexes $\{S_{\rho s}, S_{\rho W_\oplus}, S_{sW_\oplus}, S_{\rho sW_\oplus}\}$ are not visible due to their small value.

Table 4: Sobol indexes related to all the uncertain variables when $\alpha = 35\,\text{deg}$.

θ [deg]	Sobol indexes						
	S_ρ	S_s	S_{B_f}	S_{B_b}	S_{ϵ_f}	S_{ϵ_b}	$S_{W_\oplus}$
60	0.622	0.027	1.22×10^{-22}	1.88×10^{-22}	1.11×10^{-21}	6.36×10^{-21}	0.351
120	0.293	0.591	2.17×10^{-24}	3.89×10^{-24}	1.96×10^{-23}	2.09×10^{-22}	0.116
180	0.167	0.781	2.50×10^{-25}	3.28×10^{-25}	1.91×10^{-24}	2.66×10^{-23}	0.052
240	0.116	0.855	9.36×10^{-26}	1.59×10^{-25}	8.72×10^{-25}	4.59×10^{-24}	0.029
300	0.091	0.890	5.06×10^{-26}	7.03×10^{-26}	4.55×10^{-25}	3.35×10^{-24}	0.019
360	0.082	0.902	5.13×10^{-26}	8.07×10^{-26}	5.11×10^{-25}	3.13×10^{-24}	0.016

spacecraft heliocentric trajectory. This validates the results discussed in the previous subsections, where the uncertainties associated with them were neglected. As a consequence, the standard deviation of the Sun-spacecraft distance reported in Fig. 6 remains substantially unaffected, and the previous considerations are still valid.

4.4. Considerations about temperature dependance

The analysis presented so far neglects the temperature influence on the sail film optical coefficients. As a matter of fact, the experimental values reported in Tab. 3 could vary as a function of the electrical conductivity of the sail film material. During the operative phase of a solar sail-based mission, the latter depends on the sail temperature [26, 1] and consequently on the Sun-spacecraft distance r.

[27] has estimated the influence of the sail heliocentric distance on its optical properties. The obtained results highlight that the reflectivity ρ is weakly dependent on the temperature (and therefore on r), thus justifying the assumption introduced in this work. On the other hand, the emissivity coefficients ϵ_f and ϵ_b are more significantly affected by temperature variations. In particular, the total estimated effect is a combination of the emissivity increase with temperature and the augmented emitted power due to higher emissivity, which tends to reduce the sail temperature. The resulting effect can be approximated by assuming that both ϵ_f and ϵ_b scale as $r^{-2/5}$. However, since the impact of emissivity-related uncertainties turns out to be negligible, as previously discussed (see Tab. 4), the temperature dependence of the optical properties does not significantly affect this analysis, but it should only be taken into account in the determination of the sail equilibrium temperature under uncertainties.

5. Conclusions

A thorough analysis has been carried out to estimate the effects of uncertainties related to the sail optical parameters and the solar irradiance on a solar sail-based mission. The uncertainty ranges on the sail optical parameters have been quantified using recent experimental measurements, whereas the solar irradiance fluctuations have been estimated from available data provided by orbiting satellites. The uncertain parameters have been modeled as Gaussian random variables, and a generalized polynomial chaos procedure has been applied to quantify their impact on the spacecraft heliocentric trajectory. The results highlight that such an impact is negligible when the propulsive acceleration acts radially. It still remains small even in the presence of a circumferential acceleration component, and becomes important only in the case of missions requiring an accurate targeting capability. The most relevant parameter to model is the specular reflection fraction, which, according to the recent literature, takes into accounts the existence of wrinkles in the sail surface. Future research should concentrate on an estimate of the effect of uncertainties on other quantities, such as the orbital parameters, in addition to the Sun-spacecraft distance. Further investigation about the impact of solar wind particles on solar sail film properties is also advisable.

Acknowledgements

This work is supported by the University of Pisa, Progetti di Ricerca di Ateneo (Grant no. PRA_2018_44). The authors gratefully acknowledge Prof. Roman Kezerashvili for his precious comments and feedback.

References

[1] Ancona, E., Kezerashvili, R. Y., Nov. 2017. Temperature restrictions for materials used in aerospace industry for the near-Sun orbits. Acta Astronautica 140, 565–569, doi: 10.1016/j.actaastro.2017.09.002.

[2] Ancona, E., Kezerashvili, R. Y., Apr. 2019. Extrasolar space exploration by a solar sail accelerated via thermal desorption of coating. Advances in Space Research 63 (7), 2021–2034, doi: 10.1016/j.asr.2018.12.016.

[3] Bassetto, M., Niccolai, L., Quarta, A. A., Mengali, G., Feb. 2018. Logarithmic spiral trajectories generated by solar sails. Celestial Mechanics and Dynamical Astronomy 130 (2), 18.1–18.24, doi: 10.1007/s10569-017-9812-6.

[4] Battin, R., 1999. An Introduction to the Mathematics and Methods of Astrodynamics, revised Edition. AIAA Education Series, Reston, VA, Ch. 13, pp. 623–698.

[5] Braun, R. D., Powell, R. W., Engelund, W. C., Gnoffo, P. A., Nov. 1995. Mars Pathfinder six-degree-of-freedom entry analysis. Journal of Spacecraft and Rockets 32 (6), 993–1000, doi: 10.2514/3.26720.

[6] Ceriotti, M., May-Wilson, G., 2019. Can a large solar sail emulate a small one? In: The 5th International Symposium on Solar Sailing. No. 19031. Aachen, Germany, 30 July–2 August.

[7] Dachwald, B., Macdonald, M., McInnes, C. R., Mengali, G., Quarta, A. A., Jul. 2007. Impact of optical degradation on solar sail mission performance. Journal of Spacecraft and Rockets 44 (4), 740–749, doi: 10.2514/1.21432.

[8] Dachwald, B., Mengali, G., Quarta, A. A., Macdonald, M., Sep. 2006. Parametric model and optimal control of solar sails with optical degradation. Journal of Guidance, Control, and Dynamics 29 (5), 1170–1178, doi: 10.2514/1.20313.

[9] Dalla Vedova, F., Miguel, N., Colombo, C., 2019. Photonic propulsion: an option for space resources transportation to and from the Main Belt. In: The 5th International Symposium on Solar Sailing. No. 19070. Aachen, Germany, 30 July–2 August.

[10] Daukantas, P., May 2017. Breakthrough starshot. Optics and Photonic News 28 (5), 26–33, doi: 10.1364/OPN.28.5.000026.

[11] Fröhlich, C., Apr. 2006. Solar irradiance variability since 1978: Revision of the PMOD composite during solar scycle 21. Space Science Reviews 125 (1-4), 53–65, doi: 10.1007/s11214-006-9046-5.

[12] Fröhlich, C., Jul. 2012. Total Solar Irradiance observations. Surveys in Geophysics 33 (3–4), 453–473, doi: 10.1007/s10712-011-9168-5.

[13] Fröhlich, C., Lean, J., Dec. 2004. Solar radiative output and its variability: Evidence and mechanisms. Astronomy and Astrophysics Review 12 (4), 273–320, doi: 10.1007/s00159-004-0024-1.

[14] Funase, R., Shirasawa, Y., Mimasu, Y., Mori, O., Tsuda, Y., Saiki, T., Kawaguchi, J., 2011. Fuel-free and oscillation-free attitude control of IKAROS solar sail spacecraft using reflectivity control device. In: 28th International Symposium on Space Technology and Science. No. 2011-o-4-09v. Okinawa, Japan, June 5–12.

[15] Gong, S., Li, J., Nov. 2014. Solar sail heliocentric elliptic displaced orbits. Journal of Guidance, Control, and Dynamics 37 (6), 2021–2025, doi: 10.2514/1.G000660.

[16] Gong, S., Macdonald, M., Jun. 2019. Review on solar sail technology. Astrodynamics 3 (2), 93–125, doi: 10.1007/s42064-019-0038-x.

[17] Granqvist, C. G., Avendano, E., Azens, A., Oct. 2003. Electrochromic coatings and devices: survey of some recent advances. Thin Solid Films 442 (1-2), 201–211, doi: 10.1016/S0040-6090(03)00983-0.

[18] Heaton, A., Ahmad, N., Miller, K., 2017. Near earth asteroid scout thrust and torque model. In: The 4th International Symposium on Solar Sailing. No. 17055. Kyoto, Japan, 17–20 January.

[19] Heaton, A. F., Artusio-Glimpse, A. B., 2015. An update to NASA reference solar sail thrust model. In: AIAA SPACE 2015 Conference and Exposition. No. AIAA 2015-4506. Pasadena (CA), USA, August 31–September 2.

[20] Heiligers, J., Ceriotti, M., McInnes, C. R., Biggs, J. D., Jan. 2014. Mission analysis and systems design of a near-term and far-term pole-sitter mission. Acta Astronautica 94 (1), 455–469, doi: 10.1016/j.actaastro.2012.12.015.
[21] Heiligers, J., Vergaaij, M., Ceriotti, M., 2019. End-to-end trajectory design for a solar-sail-only pole-sitter at Venus, Earth, and Mars. In: The 5th International Symposium on Solar Sailing. No. 19055. Aachen, Germany, 30 July–2 August.
[22] Huang, X., Zeng, X., Circi, C., Vulpetti, G., Qiao, D., 2019. Analysis of the non-ideal solar sailing with deformation. In: The 5th International Symposium on Solar Sailing. No. 19011. Aachen, Germany, 30 July–2 August.
[23] Hughes, G. W., Macdonald, M., McInnes, C. R., Atzei, A., Falkner, P., Jul. 2006. Sample return from Mercury and other terrestrial planets using solar sail propulsion. Journal of Spacecraft and Rockets 43 (4), 828–835, doi: 10.2514/1.15889.
[24] Ishida, H., Chujo, T., Mori, O., Kawaguchi, J., 2017. Optimal design of advanced reflectivity control device for solar sails considering polarization properties of liquid crystal. In: Presentation at: The 4th International Symposium on Solar Sailing. Kyoto, Japan, 17–20 January.
[25] Jacobson, R. A., Thornton, C. L., Sep. 1978. Elements of solar sail navigation with application to a Halley's comet rendezvous. Journal of Guidance, Control and Dynamics 1 (5), 365–371, doi: 10.2514/3.55794.
[26] Kezerashvili, R. Y., Nov. 2008. Solar sail interstellar travel: 1. thickness of solar sail films. Jorunal of the British Interplanetary Society 61 (11), 430–439 .
[27] Kezerashvili, R. Y., 2014. Advances in Solar Sailing. Springer Praxis, Berlin, Ch. 3, pp. 573–592.
[28] Kopp, G., 2016. Magnitudes and timescales of total solar irradiance variability. Journal of Space Weather and Space Climate 6, A30.1–A30.11, doi: 10.1051/swsc/2016025.
[29] Kopp, G., Lean, J. L., Jan. 2011. A new, lower value of total solar irradiance: Evidence and climate significance. Geophysical Research Letters 38 (1), L01706.1–L01706.7, doi: 10.1029/2010GL045777.
[30] Lean, J. L., DeLand, M. T., Apr. 2012. How does the Sun's spectrum vary? Jounal of Climate 25 (7), 2555–2560, doi: 10.1175/JCLI-D-11-00571.1.
[31] Luo, Y., Yang, Z., Feb. 2017. A review of uncertainty propagation in orbital mechanics. Progress in Aerospace Sciences 89, 23–39, doi: 10.1016/j.paerosci.2016.12.002.
[32] Matsuno, Y., Tsuchiya, T., Wei, J., Hwang, I., Matayoshi, N., Jun. 2015. Stochastic optimal control for aircraft conflict resolution under wind uncertainty. Aerospace Science and Technology 43, 77–88, doi: 10.1016/j.ast.2015.02.018.
[33] McInnes, C. R., 1999. Solar Sailing: Technology, Dynamics and Mission Applications. Springer-Praxis Series in Space Science and Technology. Springer-Verlag, Berlin.
[34] McInnes, C. R., 2004. Delivering fast capable missions to outer Solar System. Advances in Space Research 34 (1), 184–191, doi: 10.1016/j.asr.2003.02.063.
[35] McNutt, L., Johnson, L., Kahn, P., Castillo-Rogez, J., Frick, A., 2014. Near-earth asteroid (NEA) scout. In: AIAA SPACE 2014 Conference and Exposition. No. AIAA 2014-4435. San Diego (CA), 4–7 August.
[36] Mengali, G., Quarta, A. A., Jan. 2005. Optimal three-dimensional interplanetary rendezvous using non-ideal solar sail. Journal of Guidance, Control, and Dynamics 28 (1), 173–177, doi: 10.2514/1.8325.
[37] Mengali, G., Quarta, A. A., Circi, C., Dachwald, B., Mar. 2007. Refined solar sail force model with mission application. Journal of Guidance, Control, and Dynamics 30 (2), 512–520, doi: 10.2514/1.24779.
[38] Monk, P. M. S., Mortimer, R. J., Rosseinsky, D. R., 2007. Electrochromism: Fundamentals and Applications. Wiley-VCH.
[39] Mu, J., Gong, S., Li, J., Oct. 2013. Reflectivity-controlled solar sail formation flying for magnetosphere mission. Aerospace Science and Technology 30 (1), 339–348, doi: 10.1016/j.ast.2013.09.002.
[40] Niccolai, L., Anderlini, A., Mengali, G., Quarta, A. A., Nov. 2018. Impact of solar wind fluctuation on electric sail mission design. Aerospace Science and Technology 82–83, 38–45, doi: 10.1016/j.ast.2018.08.032.
[41] Niccolai, L., Anderlini, A., Mengali, G., Quarta, A. A., Sep. 2019. Electric Sail displaced orbit control with solar wind uncertainties. Acta Astronautica 162, 563–573, doi: 10.1016/j.actaastro.2019.06.037.
[42] Niccolai, L., Bassetto, M., Quarta, A. A., Mengali, G., Apr. 2019. Solar sailing with femtosatellites: A review of smart dust architecture, dynamics, and mission applications. Progress in Aerospace Sciences 106, 1–14, doi: 10.1016/j.paerosci.2019.01.003.
[43] Niccolai, L., Quarta, A. A., Mengali, G., Mar. 2017. Analytical solution of the optimal steering law for non-ideal solar sail. Aerospace Science and Technology 62, 11–18, doi: 10.1016/j.ast.2016.11.031.
[44] Okada, T., Kebukawa, Y., Aoki, J., et al., Oct. 2018. Science exploration and instrumentation of the OKEANOS mission to a Jupiter Trojan asteroid using the solar power sail. Planetary and Space Science 161, 99–106, doi: 10.1016/j.pss.2018.06.020.
[45] Peloni, A., Dachwald, B., Ceriotti, M., Oct. 2018. Multiple near-Earth asteroid rendezvous mission: Solar-sailing options. Advances in Space Research 62 (8), 2084–2098, doi: 10.1016/j.asr.2017.10.017.
[46] Pezent, J., Sood, R., Heaton, A., 2018. Near Earth Asteroid (NEA) Scout solar sail contingency trajectory design and analysis. In: Space Flight Mechanics Meeting. No. AIAA 2018-0199. Kissimmee (FL), USA, 8–12 January.
[47] Quarta, A. A., Mengali, G., May 2011. Solar sail capabilities to reach elliptic rectilinear orbits. Journal of Guidance, Control, and Dynamics 34 (3), 923–926, doi: 10.2514/1.51638.
[48] Quarta, A. A., Mengali, G., Nov. 2013. Optimal solar sail phasing trajectories for circular orbit. Journal of Guidance, Control, and Dynamics 36 (6), 1821–1824, doi: 10.2514/1.59372.
[49] Quarta, A. A., Mengali, G., Feb. 2013. Optimal solar sail transfer to linear trajectories. Acta Astronautica 82 (2), 189–196, doi: 10.1016/j.actaastro.2012.03.005.
[50] Rios-Reyes, L., Scheeres, D. J., 2005. Robust solar sail trajectory control for large pre-launch modemodel errors. In: AIAA Guidance, Navigation, and Control Conference and Exhibit. No. AIAA 2005-6173. San Francisco (CA), USA, 15–18 August.
[51] Rottman, G., Aug. 2005. The SORCE mission. Solar Physics 230 (1–2), 7–25, doi: 10.1007/s11207-005-8112-6.
[52] Rowe, W. M., 1978. Sail film materials and supporting structure for a solar sail, a preliminary design, volume 4. Tech. rep., Jet Propulsion Laboratory, Pasadena (CA), USA.
[53] Shampine, L. F., Gordon, M. K., 1975. Computer Solution of Ordinary Differential Equations: The Initial Value Problem.

W. H. Freeman, San Francisco, Ch. 10, ISBN: 978-0716704614.
[54] Shampine, L. F., Reichelt, M. W., Jan. 1997. The MATLAB ODE suite. SIAM Journal on Scientific Computing 18 (1), 1–22, doi: 10.1137/S1064827594276424.
[55] Sobol, I. M., Feb. 2001. Global sensitivity indices for nonlinear mathematical models and their Monte Carlo estimates. Mathematics and Computers in Simulation 55 (1-3), 271–280, doi: 10.1016/S0378-4754(00)00270-6.
[56] Sokół, J. M., Bzowski, M., Tokumaru, M., Fujiki, K., McComas, D. J., Jul. 2013. Heliolatitude and time variations of solar wind structure from in situ measurements and interplanetary scintillation observations. Solar Physics 285 (1-2), 167–200, doi: 10.1007/s11207-012-9993-9.
[57] Tsuda, Y., Mori, O., Funase, R., Sawada, H., Yamamoto, T., Takanao, S., Endo, T., Yonekura, K., Hoshino, H., Kawaguchi, J., 2011. Achievement of IKAROS - Japanese deep space solar sail demonstration mission. In: Presentation at: 7th IAA Symposium on Realistic Advanced Scientific Space Missions. Aosta, Italy, 11–13 July.
[58] Valli, M., Armellin, R., Di Lizia, P., Lavagna, M. R., Jan. 2013. Nonlinear mapping of uncertainties in celestial mechanics. Journal of Guidance, Control, and Dynamics 36 (1), 48–63, doi: 10.2514/1.58068.
[59] Vulpetti, G., Jul. 2010. Effect of the total solar irradiance variations on solar-sail low-eccentricity orbits. Acta Astronautica 67 (1–2), 279–283, doi: 10.1016/j.actaastro.2010.02.004.
[60] Vulpetti, G., Mar. 2011. Total solar irradiance fluctuation effect on sailcraft-mars rendezvous. Acta Astronautica 68 (5–6), 644–650, doi: 10.1016/j.actaastro.2010.01.010.
[61] Vulpetti, G., 2013. Fast Solar Sailing: Astrodynamics of Special Sailcraft Trajectories. Springer Netherlands, Ch. 3, p. 89.
[62] Wang, W., Mengali, G., Quarta, A. A., Yuan, J., Sep. 2017. Formation flying for electric sails in displaced orbits. part i: Geometrical analysis. Advances in Space Research 60 (6), 1115–1129, doi: 10.1016/j.asr.2017.05.015.
[63] Wang, W., Mengali, G., Quarta, A. A., Yuan, J., Sep. 2017. Formation flying for electric sails in displaced orbits. part ii: Distributed coordinated control. Advances in Space Research 60 (6), 1130–1147, doi: 10.1016/j.asr.2017.06.017.
[64] Wright, J. L., 1992. Space Sailing. Gordon and Breach Science Publishers, Philadelphia, PA.
[65] Xiu, D., Karniadakis, G. E., Oct. 2003. The Wiener–Askey Polynomial Chaos for stochastic differential equations. SIAM Journal of Scientific Computing 24 (2), 619–644, doi: 10.1137/S1064827501387826.
[66] Zeng, X., Vulpetti, G., Circi, C., Mar. 2019. Solar sail H-reversal trajectory: A review of its advances and applications. Astrodynamics 3 (1), 1–15, doi: 10.1007/s42064-018-0032-y.